International Journal of Thermofluids 20 (2023) 100442

Contents lists available at ScienceDirect

International Journal of Thermofluids

journal homepage: www.sciencedirect.com/journal/international-journal-of-thermofluids

Energy and exergetic performance analysis of a hybrid solar multi-stage Brayton cycle with different working fluids

Faustino Moreno-Gamboa [a], César Nieto-Londoño [b,*]

[a] Facultad de Ingeniería, Grupo de Fluidos y Térmicas, Universidad Francisco de Paula Santander, Cúcuta Colombia
[b] Escuela de Ingeniería, Grupo de Energía y Termodinámica, Universidad Pontifica Bolivariana, Medellín Colombia

ARTICLE INFO

Keywords:
CSP Brayton cycle
Exergy analysis
Energy systems analysis
Working fluids

ABSTRACT

An energy and exergy model for a hybrid multi-stage Brayton cycle solar thermal plant is presented, incorporating an arbitrary number of compression stages with intermediate cooling and expansion with reheating. In hybrid operation, the cycle receives thermal energy from a solar concentration system of a heliostat field and a central tower complemented by reheaters and an external main combustion chamber of natural gas. The proposed model considers the irreversibility of the plant's components, and direct solar radiation is estimated with the Daily Integration Approach model. The model is validated and implemented with the Solugas experimental plant parameters and is applied in Barranquilla, Colombia. Additionally, this work presents a comparative analysis of different plant configurations using air, carbon dioxide and helium as working fluids. Comparing the power, the energetic and exergetic efficiencies, and the destruction of exergy on an average day of the year, the maximum points of these variables are also found as a function of the pressure ratio. Observing that the two-compression-one-expansion CO_2 cycle presents maximum fuel conversion rates and the slightest destruction of total exergy.

1. Introduction

Energy demands and concerns about polluting emissions and climate change effects are constantly growing. In this sense, great efforts are required to develop technologies that convert energy with low environmental impacts. For instance, wind energy has found its best performance so far in three-blade turbines; however, the high rate of land occupation and the substantial variations in the wind resource prediction still has to be improved [1]. On the other side, solar energy is gaining space in the energy mix, being solar PV systems the most widely implemented worldwide [2]. However, solar thermal power plants are an alternative due to the possibility of continuous power generation when coupled with thermal storage facilities [3] or hybridised with different heat sources [4].

Regarding the most used power cycle configurations, steam cycles (i.e. Rankine and Organic Rankine cycles) are the most widely implemented in solar thermal plants. Although, steam power cycles require extensive cooling systems and available water for operation [5]. Contrary to those, Brayton cycle plants are presented as an excellent option given the reduced cooling water requirement, the possibility of using different fuels, the implementation of hybridisation mechanisms with solar concentration systems, and the application of other working fluids [6]. Concentrated Solar Power (CSP) systems applied in power plants are presented as a viable option for diversifying the world energy mix. The installed capacity of CSP systems has increased from 1.2 GW in 2010 to 6.2 GW in 2020 [7]. Furthermore, combining CSPs and gas turbines may be technically feasible due to the possibility of operating at temperatures above 1000 °C, more comprehensive power output ranges, and simple cycles [8]. Currently, these systems are not commercially available and are under development. Experimental Brayton cycle solar thermal power plants are Solugas in Sevilla, Spain [9] and Sciro in Australia [10].

Regarding efficiency, there is still room to work on Brayton's cycle performance. In this regard, the efficiency of this kind of cycle can be improved by reducing the intake air temperature and modifying the combustion chamber to have the best air-fuel ratio [11].

Additionally, regenerators are used under different conditions, even at high temperatures, increasing operation performance by harvesting waste heat rejected [12,13]. On the other hand, several compression stages with intermediate cooling steps and different configurations with expansion stages with intermediate reheating have been studied [14,15]. It was found that the maximum power output is obtained if the reheating is installed at 40% of the expansion section and the

* Corresponding author.
E-mail address: cesar.nieto@upb.edu.co (C. Nieto-Londoño).

https://doi.org/10.1016/j.ijft.2023.100442

Available online 10 August 2023

Nomenclature

A_o	Heliostat field area, m^2
A_r	Area of incidence in the central receiver, m^2
$\overline{D}_h$	Monthly average daily diffuse radiation, kWh/m^2 /day
e	Exergy specified at the input or output of each component.
$\dot{E}_{d,a}$	Exergy destroyed in the ambient heat exchanger, kW
$\dot{E}_{d,cm}$	Exergy destroyed in the compressor, kW
$\dot{E}_{d,cc}$	Exergy destroyed in the combustion chamber, kW
$\dot{E}_{d,ccr}$	Exergy destroyed in the reheaters, kW
$\dot{E}_{d,\ he}$	Exergy destroyed in the Heliostat field, kW
$\dot{E}_{d,r}$	Exergy destroyed in the regenerator, kW
$\dot{E}_{d,re}$	Exergy destroyed in the receiver, kW
$\dot{E}_{d,tm}$	Exergy destroyed in the turbine, kW
$\dot{E}_{in}$	Exergy input to the solar concentrator, kW
$\overline{H}_h$	Monthly average daily global radiation, kWh/m^2 /day
I_h	Global solar radiation, W/m^2
I_{bh}	Direct solar radiation, W/m^2
I_{dh}	Diffuse solar radiation, W/m^2
$\dot{m}$	Working fluid mass flow rate, kg/s.
$\dot{m}_f$	Fuel mass flow in the main combustion chamber, kg/s
$\dot{m}_{fr}$	Fuel mass flow in reheaters, kg/s
N_c	Number of compressors
N_t	Number of turbines
$\dot{W}_{net}$	Net power output, kW
Q_{hlv}	Lower heating value of fuel, kJ/kg
$\dot{Q}_{ae}$	Heat output to the intercoolers, kW
$\dot{Q}_h$	Total heat absorbed by the working fluid, kW
$\dot{Q}_{hc}$	Heat input from the combustion chamber, kW
$\dot{Q}_{hct}$	Heat input to the combustion chamber heat exchanger, kW
$\dot{Q}_{hcr}$	Heat input to the reheaters, kW
$\dot{Q}_{hs}$	Heat input from the solar concentrator, kW
$\dot{Q}_{hst}$	Heat input to the solar receiver heat exchanger, kW
$\dot{Q}_r$	Heat supplied by the Heliostat field, kW
$\dot{Q}_p$	Heat loss in the solar receiver, kW
$\dot{Q}_l$	Heat transferred to the environment, kW
r_d	Diffuse radiation hour/day ratio
r_c	Compressor pressure ratio
r_p	Overall pressure ratio
r_t	Turbine pressure ratio
r_g	Global solar radiation hour/day ratio
T_{hs}	Solar receiver operating temperature, K
T_{hc}	Combustion chamber operating temperature, K
U_L	Overall receiver loss parameter, W/ m^2 K
$\dot{W}_c$	Compressor power consumption, kW
$\dot{W}_t$	Power generated by the turbine, kW
η	Overall cycle efficiency
η_c	Compressor isentropic efficiency
η_t	Isoentropic efficiency of the turbine
η_o	Heliostat field optical efficiency
ε_{is}	Solar receiver heat exchanger effectiveness
ε_{ic}	Combustion chamber heat exchanger effectiveness
ε_l	Heat exchanger surrounding effectiveness
U_L	Conduction–convection heat transfer coefficient, W/ m^2 K

intermediate cooling is at 50% of the compression section [16]. Other studies suggest using lower cycles and mechanisms such as water or steam injection in gas turbine cycles [17] and the development of combined cycles with gas and steam turbines. These systems are handy for generation capacities more significant than 50 MW.

Some studies of CSPs with gas turbines have considered combustion chamber hybridisation systems. The hybrid system allows for maintaining the turbine's operation without being affected by the changes in the solar resource, reaching study prototypes with solar input up to 70% [18]. Models have been developed to predict the performance of hybrid CSP Brayton plants [19], applied on representative days of each season in Seville, Spain, finding that the fuel savings of a hybrid plant can vary between 4% on a representative day in winter and 12% on a representative summer day [20]. Another mechanism to improve the performance of Brayton solar cycles is the steam injection, whose efficiency ranges between 45% and 55%, and the solar fraction increases up to 50% [21]. Finally, some combined cycles have also been evaluated with solar concentration systems as energy input in both cycles, achieving improved efficiency in places of high temperatures and low humidity [22].

The typical Brayton cycle operates with air as the primary working fluid; however, other working fluids are studied to replace it and improve gas turbines' performance. Helium has a specific heat constant pressure four times higher than air and can operate with higher energy transfers [23]. It is estimated that, compared to an air cycle, the helium gas turbine could take advantage of the high temperature and generate electricity efficiently [24]. A closed energy conversion system with a Brayton cycle operating with helium was developed in Germany. Two systems were created to explore using helium as a working fluid in gas turbines: the first was composed of a heater, a turbine, a compressor and related equipment whose power is 50 MW. The second was a high-temperature plant to test the helium compressor and other components used in a direct cycle system [25]. A third attempt was implemented in China, where a pilot project was developed in 2003 with a gas turbine and a 10 MW helium-cooled high-temperature reactor [26].

On the other hand, supercritical carbon dioxide cycles represent an alternative to Brayton's working fluid due to its high density near the critical point, which implies less compression work and, therefore, greater cycle efficiency [27]. However, these cycles are limited to low-pressure ratios due to the maximum pressure on commercial equipment [28]. Therefore, the use of carbon dioxide under subcritical conditions has also been evaluated, and higher values of heat transfer coefficients have been observed [29], achieving reductions in fuel consumption and an increase in cycle efficiency [30].

Generally, studies in the literature are intended to analyse particular power plant configurations. However, models have been developed that evaluate different Brayton cycle configurations where efficiency and power output increase with the increase of expansion and compression stages [31]. Subsequently, a model is evaluated in different plant configurations from a design solar radiation value and variable specific heats [23]. However, the developed multi-stage models do not present exergy destruction models for arbitrary expansion and compression stages.

In the revision of the state-of-art, the current state of gas turbines and their capability to be used in solar concentration systems with a Brayton cycle was stated. Additionally, a review of several works showing the application of gas turbines using different working was presented, where carbon dioxide in subcritical and supercritical conditions stand out among others. The use of helium in gas turbine systems, with its strengths and weaknesses, was also reviewed. Although some of the studies reviewed have similarities with the present work's aim, neither can perform energy and exergy analysis of a solar hybrid system, including several cycle configurations regarding the number of compression and expansion stages and implementing a heat regenerator within the same thermodynamic model. Additionally, the model

implemented has the versatility to evaluate the cycle's energy and exergetic performance operating with several working fluids and considering the site's atmospheric conditions over different days of the year.

Considering the previous, the main objective of this paper is to present and evaluate an energy and exergy analysis model of hybrid Brayton cycle solar power plants for an arbitrary number of compression stages with intermediate cooling and expansion stages with intermediate reheating. The work is presented in several sections described below: Section 2 describes the models used in this work, starting with the solar radiation model that allows hourly radiation based on monthly average daily values. Next, a thermodynamic energy and exergy model of a closed Brayton hybrid solar plant is developed for arbitrary compression and expansion stages, using irreversibilities in the compression, expansion and heat transfer processes. Finally, the exergy destruction models for the different components of the system are presented. In Section 3, the solar resource and thermodynamic models are validated from data reported in the literature for a plant with similar conditions. In Section 4, the simulation of the operation of the plant in different configurations is performed for the environmental-specific conditions in Barranquilla, Colombia. A comparative evaluation of the evolution of different energy and exergetic parameters during the day for different hybrid solar configurations is developed. The maximum values of power and efficiency are estimated according to the pressure ratio for different working fluids.

2. Models and plant layout

This section describes the models used for evaluating the performance of a multi-stage Brayton Cycle power plant. First, the Daily Integration (DI) model evaluated direct solar irradiation regarding Colombian conditions. Then, a plant scheme with a multi-stage Brayton Cycle is presented, including the thermodynamic models used for the energy and exergy analysis performed.

2.1. Direct solar radiation model

The Daily Integration (DI) model developed by Gueymard [32] allows finding the values of direct solar radiation (I_{bh}) as follows,

$$I_{bh} = r_g \overline{H}_h - r_d \overline{D}_h, \tag{1}$$

where, the hour-to-day ratios for diffuse radiation (r_d) and global radiation (r_g) are introduced. Additionally, ($\overline{D}_h$) and ($\overline{H}_h$) represent the long-term average daily total and diffuse irradiation, respectively. Details of the daily integration model and its application can be found in [32,33]. The DI model was previously assessed and fitted in good agreement with the experimental data results [34].

2.2. Brayton solar hybrid multi-stage power plant energy model

The inclusion of an arbitrary number of turbines N_t and compressors N_c in a hybrid solar Brayton cycle, Fig. 1 shows that the main combustion chamber and the solar concentrating system share the heat supply to the power cycle to reach the conditions of entry to the first turbine. Additionally, Fig. 2 shows the temperature-entropy diagram for the multi-stage plant. It is also observed that each compressor has an intermediate cooling, and each turbine has an intermediate reheating.

The operation of the plant presented in Fig. 1 can be described as follows: the working fluid starts the cycle in state 1 (T_1,p_1), which passes through several N_c compressors to compress the working fluid to state 2. At this point, $N_c - 1$ intermediate cooling is required, reducing the working fluid temperature to T_1, the inlet of the subsequent compressor. The intermediate cooling process is considered isobaric. At the outlet of the last compressor N_c, the working fluid passes through the regenerator and receives heat from the working fluid leaving the last turbine N_t (process 2–3). Subsequently, a solar receiver (process 3–4) receives the concentrated irradiation from the heliostat field and delivers heat to the air through a heat exchanger. This is followed by a combustion chamber (process 4–5) that burns natural gas and delivers heat to the air through a heat exchanger. After leaving the main combustion chamber, the working fluid passes through a number N_t turbines, where it expands to state 6. Here, a number $N_t - 1$ of intermediate reheating is required, which should again bring the working fluid up to temperature T_5 at the inlet of the next turbine. The reheating process is considered to be isobaric. Finally, the working fluid passes through the regenerator to reach state 7 and enters the heat exchanger, which brings it back to temperature T_1 to restart the cycle.

The thermodynamic model developed considers that to reduce power losses in the compression stages and maximise power output in the expansion stages, the pressure ratios of all compressors and turbines must be equal [35]. Therefore, as shown in Fig. 2, for each of the N_c

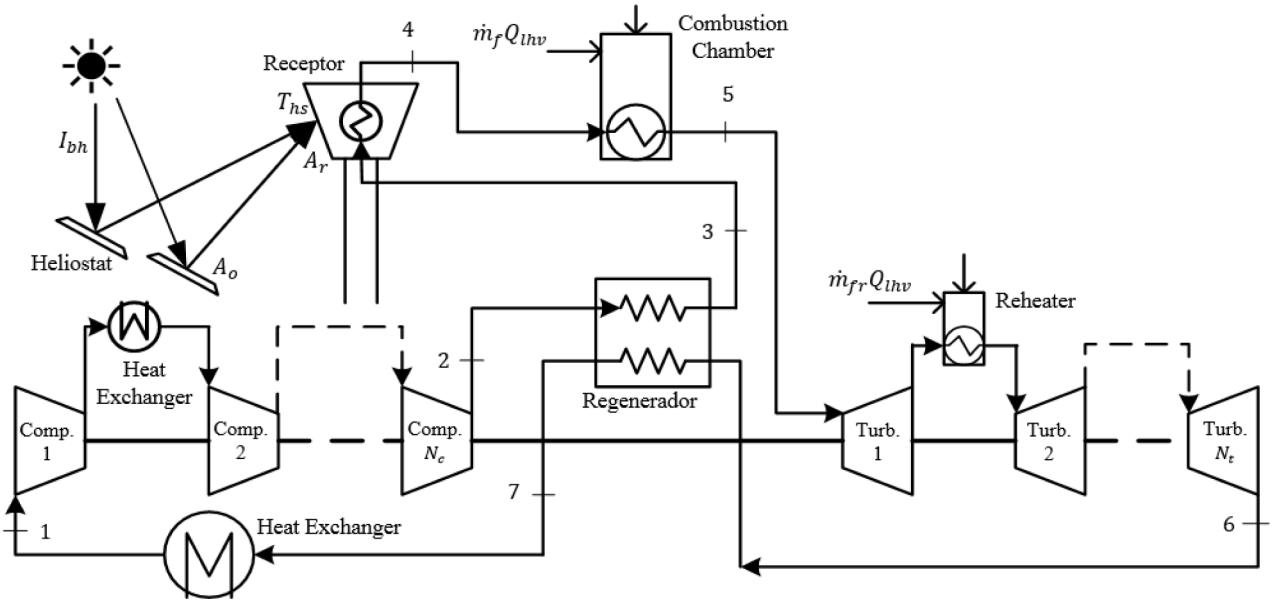

Fig. 1. Schematic of the hybrid solar plant with an arbitrary number of compressors and turbines.

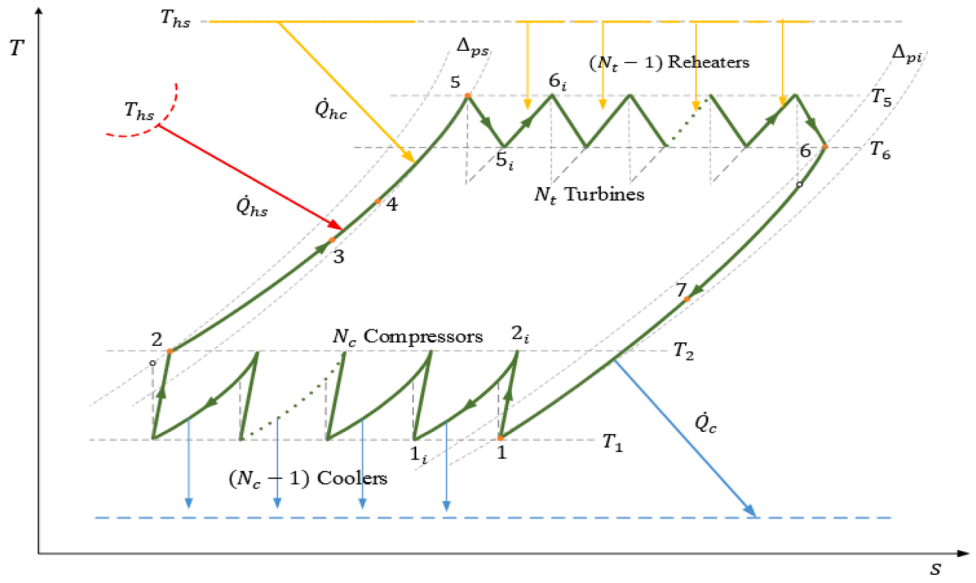

Fig. 2. Temperature-entropy diagram for the multi-stage plant.

turbines, the inlet temperature is T_1 and the outlet temperature is T_2; likewise, for each of the $N_t$turbines, the inlet temperature is T_5 and the outlet temperature is T_6. In this sense, the compression ratio $N_c$can be defined starting from an overall plant pressure ratio $r_p$as follows,

$$r_c = p_{2i} \Big/ p_1 = r_p^{1/N_c} \tag{2}$$

According to the system diagram, the energy balance in the compressor is expressed as,

$$\dot{W}_c = \dot{m}(h_{2i} - h_1), \tag{3}$$

$$\eta_c = (h_{2is} - h_1)/(h_{2i} - h_1), \tag{4}$$

where $\dot{W}_c$ represents the power required by the compressor, $r_p$is the overall pressure ratio of the cycle, $r_c$is the compressor's pressure ratio, $\dot{m}$ is the air mass flow rate, $\eta_c$is the isentropic efficiency of the compressor, and h is the enthalpy in each defined state. Note that for $N_c = 1$ h_{2i} is the same h_2.

Similarly, the compression ratio for each turbine must be defined from the global pressure ratio r_p. For this, the pressure drops in the heat transfer processes are considered associated with each component (processes 2–5 and 6–1); therefore, the lines in Fig. 2 are not continuous. In order to evaluate the pressure losses, overall loss coefficients D_{ps} in the heat supply process (process 2–5) and D_{pi} in the heat expulsion process (process 6–1) are defined, as shown in Fig. 2. These coefficients are according to [30,31],

$$D_{ps} = \left(P_s - \Delta_{ps}\right)/P_s, \tag{5}$$

$$D_{pi} = \left(P_i - \Delta_{pi}\right)/P_i, \tag{6}$$

where, $P_s$andP_i represent the upper and lower pressure of the cycle and Δ_p represents the pressure drops according to Fig. 2. Therefore, the pressure losses in the heat addition and extraction processes are considered at the turbine's inlet and outlet, respectively. Hence, the pressure ratio of each turbine is:

$$r_t = \frac{p_5}{p_{6is}} = \left(D_{ps}\, D_{pi}\, r_p\right)^{(1/N_t)}. \tag{7}$$

The energy balance and isentropic efficiency η_t of the turbine are described below, where $\dot{W}_t$ is the turbine power rate and r_t is the turbine's pressure ratio,

$$\dot{W}_t = \dot{m}(h_5 - h_{6i}), \tag{8}$$

$$\eta_t = \frac{(h_6 - h_5)}{(h_{6s} - h_5)}. \tag{9}$$

Note that for $N_t = 1$ $h_{6i}$is the same as h_6. The above allows defining a relationship for the net cycle power rate $\dot{W}_{net}$, as a function of an arbitrary number of compression stages N_c and expansion stages N_t, as follows,

$$\dot{W}_{net} = (N_t\, \dot{m}(h_5 - h_{6i})) - (N_c\, \dot{m}(h_{2i} - h_1)), \tag{10}$$

The regenerator supplies heat to the air leaving the compressor from the energy available in the air exhausting at the turbine only if the conditional $T_6 > T_2$ is satisfied. Moreover, the effectiveness of the regenerator is as follows,

$$\varepsilon_r = \frac{(h_3 - h_2)}{(h_6 - h_2)} = \frac{(h_7 - h_6)}{(h_2 - h_6)}. \tag{11}$$

After passing through the compressor, the working fluid receives three heat additions. The first of these occurs in the regenerator, as explained before; the second heat addition occurs in the solar concentration system, in which initially, the solar radiation is received by the heliostat field, which reflects the heat $\dot{Q}_r$ reaching the receiver of the central tower, presenting heat losses heat $\dot{Q}_p$ such that the heat available at the receiver is $\dot{Q}_{hst}$. The above is estimated as,

$$\dot{Q}_r = \eta_0\, A_o\, I_{bh}, \tag{12}$$

$$\dot{Q}_{hst} = \dot{Q}_r - \dot{Q}_p, \tag{13}$$

where η_0 is the heliostat field's optical efficiency depends on cosine efficiency losses, surface quality, cleanliness, tracking system, and reflectivity. Since this work's objective is not to estimate this efficiency, a global efficiency of the heliostat field reported in the literature will be used [36].

On the other hand, the heat losses in the receiver $\dot{Q}_p$ can be evaluated by assigning linear values of the temperature difference for convection and conductive losses and non-linear values for radiation losses [37]. In this case, the analysis is performed according to the definition of losses in the central receiver as follows,

$$\dot{Q}_p = A_r\left(h_w(T_{hs} - T_0) + U_{cond}(T_{hs} - T_0) + \alpha\sigma\left(T_{hs}^4 - T_0^4\right)\right), \tag{14}$$

where $T_{hs}$is the central receiver temperature, $h_w$and $U_{cond}$are respectively the convective and conductive heat transfer coefficients, α is the central receiver surface emissivity, σ is the Stefan-Boltzmann constant and $A_r$is the receiver area. In the above relation, a conductive and convection heat transfer coefficient U_l is included, thus expressing $\dot{Q}_p$ as,

$$\dot{Q}_p = A_r\left(U_l(T_{hs} - T_0) + \alpha\sigma\left(T_{hs}^4 - T_0^4\right)\right). \tag{15}$$

The receiver delivers heat, $\dot{Q}_{hs}$, to the working fluid (process 3–4), through a heat exchanger with effectiveness ε_{is} [19,38]; both defined below as,

$$\varepsilon_{is} = (T_4 - T_3)/(T_{hs} - T_3), \tag{16}$$

$$\dot{Q}_{hs} = \varepsilon_{is}\ \dot{Q}_{hst} = \dot{m}\ (h_4 - h_3). \tag{17}$$

The above expressions allow evaluation of the efficiency of the concentrating solar power system as follows,

$$\eta_s = \frac{\left(\dot{Q}_r - \dot{Q}_p\right)}{(I_{bh}\ A_o)}. \tag{18}$$

Replacing Eqs. (31) and (33) in (34) and solving for η_s, the following equation is obtained

$$\eta_s = \eta_0 - \frac{U_l(T_{hs} - T_0)}{(I_{bh}(A_o/A_r))} - \frac{\alpha\sigma\left(T_{hs}^4 - T_0^4\right)}{(I_{bh}(A_o/A_r))}. \tag{19}$$

The third and final process of heat delivery to the working fluid (process 4–5) occurs in the combustion chamber, as follows,

$$\dot{Q}_{hct} = \eta_{cc}\ Q_{lhv}\ \dot{m}_f, \tag{20}$$

where $\dot{Q}_{hct}$ is the heat available in the chamber, η_{cc} is the combustion chamber efficiency, Q_{lhv} is the lower heating value of the fuel, and $\dot{m}_f$ is the fuel's mass flow rate. As in the case of the receiver, heat is delivered to the working fluid, $\dot{Q}_{hc}$, in the combustion chamber using a heat exchanger with effectiveness ε_{is} [19,38], defined as,

$$\dot{Q}_{hc} = \varepsilon_{ic}\ \dot{Q}_{hct} = \dot{m}\ (h_5 - h_4), \tag{21}$$

$$\varepsilon_{ic} = \frac{(T_5 - T_4)}{(T_{hc} - T_4)}. \tag{22}$$

Similarly, the fuel consumption of each reheater, $\dot{m}_{fr}$ and the total fuel consumed by the $(N_t - 1)$ reheaters, $\dot{m}_{frt}$, is expressed as,

$$\dot{m}_{fr} = (\dot{m}(h_{5i} - h_{6i}))/(\varepsilon_{hc}\ \eta_{cc}\ Q_{lhv}), \tag{23}$$

and,

$$\dot{m}_{frt} = (N_t - 1)\ \dot{m}_{fr} \tag{24}$$

On the other hand, the values of $\dot{Q}_{hs}$ and $\dot{Q}_{hc}$ represent the external heat delivered to the working fluid by the solar concentrating system and the combustion chamber. Meanwhile $\dot{Q}_{hcr}$ represents the heat supplied by the $(N_t - 1)$ reheaters. Therefore, $\dot{Q}_h$ is defined as the total heat supplied to the working fluid and is expressed as

$$\dot{Q}_h = \dot{Q}_{hc} + \dot{Q}_{hs} + \dot{Q}_{hsr}. \tag{25}$$

The heat supplied by the reheaters is defined by

$$\dot{Q}_{hsr} = (N_t - 1)\ \dot{m}(h_{5i} - h_{6i}). \tag{26}$$

The definition of the heat input makes it possible to determine the solar fraction, which is the fraction of the solar heat received by the working fluid, expressed as,

$$f = \dot{Q}_{hs}/\dot{Q}_h. \tag{27}$$

Additionally, the cycle transfers heat to the environment, $\dot{Q}_a$, with an effectiveness ε_l [19,20] and the heat delivered by the $(N_c - 1)$ intermediate coolings, $\dot{Q}_{ae}$, expressed as,

$$\dot{Q}_a = \dot{m}\ (h_7 - h_1), \tag{28}$$

$$\varepsilon_l = \frac{(T_1 - T_7)}{(T_0 - T_7)}, \tag{29}$$

$$\dot{Q}_{ae} = (N_c - 1)\dot{m}(h_{2i} - h_{1i}). \tag{30}$$

The overall efficiency of the plant is

$$\eta = \dot{W}_{net}/\left(\left(\dot{m}_f + \dot{m}_{frt}\right)Q_{lhv} + (I_{bh}\ /\ 1000)A_o\right), \tag{31}$$

and the thermal engine efficiency can be expressed as,

$$\eta_h = \dot{W}_{net}/(\dot{m}((h_3 - h_5) - T_0(s_3 - s_5)) + \dot{m}(N_t - 1)((h_{5i} - h_{6i}) - T_0\ (s_{5i} - s_{6i}))), \tag{32}$$

Finally, the fuel conversion rate of the plant is defined as the power generated over the energy of the fuel consumed [20],

$$r_e = \dot{W}_{net}/\left(\left(\dot{m}_f + \dot{m}_{frt}\right)Q_{lhv}\right). \tag{33}$$

The fuel conversion rate allows considering the effect of fuel consumption and its impact on operating costs.

2.3. Hybrid solar thermal plant exergy model

This section presents the exergy models for which the exergy balance is proposed for each component. It is worth noting that the kinetic and potential exergy changes and the components' chemical exergy are neglected. First, the general exergy balance equation is reduced for a single, steady flow system [39]. Subsequently, the standard equations for the exergy destruction of the components, such as compressors (34), turbines (35), and regenerators (36), are described as follows:

$$\dot{E}_{d,cm} = N_c\ [\dot{m}((h_1 - h_{2i}) - T_0(s_1 - s_{2i})) + \dot{W}_c], \tag{34}$$

$$\dot{E}_{d,tm} = N_t\ [\dot{m}((h_5 - h_{6i}) - T_0(s_5 - s_{6i})) - \dot{W}_t], \tag{35}$$

$$\dot{E}_{d,r} = \dot{m}((h_6 - h_7 + h_2 - h_3) - T_0(s_6 - s_7 + s_2 - s_3)), \tag{36}$$

Additionally, as the cycle dissipates heat to the environment, the exergy destruction is evaluated as

$$\dot{E}_{d,a} = \dot{m}((h_7 - h_1) - T_0(s_1 - s_2)). \tag{37}$$

Considering that the system can have $N_c - 1$ coolings, the destruction of exergy of each cooling and the total of them is calculated as follows,

$$\dot{E}_{d,ae} = (N_c - 1)[\dot{m}\ ((h_{2i} - h_{1i}) - T_0\ (s_{2i} - s_{1i}))]. \tag{38}$$

Additionally, it is required to estimate the exergy destruction in the combustion chamber and reheaters as described by Moreno-Gamboa and Nieto-Londoño [4]. For this purpose, the analysis of the exergy balance in a control volume containing both the combustion chamber and its heat exchanger is simplified [4], and the flows of air $\dot{m}_a$ and fuel $\dot{m}_f$ and $\dot{m}_{fr}$ for combustion are defined as inputs and the combustion product gases as outputs $(\dot{m}_a + \dot{m}_f)$. In addition, the working fluid from the receiver enters state 4 and leaves state 5. Also, the same analysis is performed for each reheater between states 6_i and 5_i.

The destruction of exergy for the main combustion chamber and the $(N_t - 1)$ reheaters are:

$$\dot{E}_{d,cc} = \dot{m}_a E_{m,a} + \dot{m}_f\ E_{m,f} - \left(\dot{m}_a + \dot{m}_f\right)E_{m,g} + \dot{m}\ ((h_4 - h_5) - T_0\ (s_4 - s_5)), \tag{39}$$

$$\dot{E}_{d,ccr} = (N_t - 1)\left[\dot{m}_a E_{m,a} + \dot{m}_{fr}\ E_{m,f} - \left(\dot{m}_a + \dot{m}_{fr}\right)E_{m,g} + \dot{m}\ ((h_{6i} - h_{5i}) - T_0\ (s_{6i} - s_{5i}))\right], \tag{40}$$

where $E_{m,a}$, $E_{m,f}$ and $E_{m,g}$ are the specific exergy of air, fuel and exhaust gases, respectively. The above specific exergy values are estimated from a relation for mixtures described as $E_m = E_q/M_m$ [40], where $M_m$represents the molar mass of the mixture and E_q is the chemical exergy of the natural gas, air or combustion products, which are estimated by the following expression,

$$E_q = \sum_{i=1}^{j} y_i E_i + R_g T_0 \sum_{i=1}^{j} y_i Ln(y_i), \tag{41}$$

where $y_i$is the molar fraction of each fuel component, $E_i$the specific exergy of the fuel component, R_g the universal gas constant. Therefore, it is possible to determine the exergy of the combustion chamber exit gases, fuel, and air entering the combustion chamber.

For the concentrating solar power system, the total solar energy input to the system is defined based on the maximum useful work available as a function of the radiation, according to [41],

$$\dot{E}_{x,s} = \frac{I_{bh}}{1000} A_o \left[1 + \frac{1}{3}\left(\frac{T_0}{T_s}\right)^4 - \frac{4}{3}\frac{T_0}{T_s}\right]. \tag{42}$$

The total exergy received by the receiver from the heliostat field is

$$\dot{E}_{x,i} = \dot{Q}_r \left(1 - \frac{T_0}{T_{hs}}\right). \tag{43}$$

Therefore, the exergy destroyed by the heliostat field is [49],

$$\dot{E}_{d,he} = \dot{E}_{x,s} - \dot{E}_{x,i}. \tag{44}$$

For the solar receiver, the exergy destruction is expressed as,

$$\dot{E}_{d,rc} = \dot{Q}_{hs1}\left(1 - \frac{T_0}{T_{hs}}\right) + \dot{m}((h_3 - h_4) - T_0(s_3 - s_4)). \tag{45}$$

The total exergy destroyed by the solar thermal plant $\dot{E}_{d,T}$, the global exergy efficiency η_{ex} and the thermal exergy efficiency $\eta_{exh}$are defined as,

$$\dot{E}_{d,T} = \dot{E}_{d,cm} + \dot{E}_{d,tm} + \dot{E}_{d,r} + \dot{E}_{d,a} + \dot{E}_{d,ae} + \dot{E}_{d,cc} + \dot{E}_{d,ccr} + \dot{E}_{d,he} + \dot{E}_{d,rc}, \tag{46}$$

$$\eta_{ex} = \dot{W}_{net}/\left(\dot{E}_{x,s} + \left(\dot{m}_f + \dot{m}_{frt}\right)E_{m,f}\right), \tag{47}$$

Finally, the destruction fraction of each component can be estimated using $FE_{d,j} = \dot{E}_{d,j}/\dot{E}_{d,T}$.

The model is implemented in the Dymola compiler based on the Modelica language. By default, Modelica transforms the model into an ODE representation to perform a simulation using numerical integration methods, where the solution is attained after the convergence has been obtained. The default solver, DASSL, is used due to its ability to be an implicit, higher-order and multi-step solver with a step-size control, which is relatively stable for a wide range of models. The simulation is performed every hour in a 24 h interval.

3. Validation of the solar and thermodynamic models, selection of the simulation site and description of the working fluids

This section presents the assessment of the solar resource and thermodynamic models. The third section also describes the cycles defined for the simulation as a function of the working fluids to be evaluated.

3.1. Validation of the solar model

The daily integration model is validated using San Lucar La Mayor, Seville, Spain information. At that specific site, the global radiance value is $\overline{H}_h = 7.8$ kWh/m^2/day and diffuse is $\overline{D}_h = 1.7$ kWh/m^2/day [42]. Fig. 3 shows the I_{bhc} values obtained with the model (red circles) and I_{bhm}measured throughout the day in Seville (blue triangles) taken from the Meteosevilla database for the same day [43].

Following the methodology proposed in [44–46], the values obtained with the DI model and those reported by the San Lucar station are compared by calculating Mean Absolute Bias Error (MABE) in order to estimate the fitting of the implemented model. The MABE provides long-term performance information correlations by comparing the actual deviation between the calculated and measured values through the absolute value of their difference. In addition, the Root Mean Square Error (RMSE) is estimated to provide short-term information. The MABE and RMSE values obtained agree with those reported in the literature, where valuations of solar resource models are performed. For the DI model, the value $MABE = 0.201085$ is within the range of 0 – 0.212 of Yao et al. [45], and for $RMSE = 0.226616$ is within the range of 0 – 0.329 [44,45].

3.2. Validation of the thermodynamic model for the hybrid solar thermal plant

The thermodynamic model with several compression stages, including intermediate cooling and expansion with intermediate reheating validation, is performed using results reported by Sanchez Orgaz [47]. In that work, a hybrid multi-stage energy model was developed for a solar concentration system. Results of the model were compared with those of an R&D project by the European Community [48,49], where several thermodynamic cycles were analysed to choose the most suitable cogeneration system design with capacities up to 500 kW. The project concluded that the two-compressor cycle with intermediate cooling is the most suitable at pressure ratios around 6, presenting a lesser airflow requirement.

Given the above, the validation is performed with two compressors and one turbine, where the following operating conditions are taken for

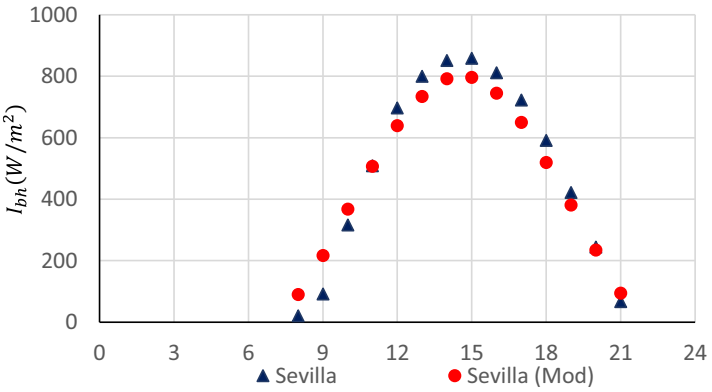

Fig. 3. Evaluación del modelo DI de radiación solar.

the plant: pressure ratio of $r_p = 6$, mass flow rate $\dot{m} = 1.97$ kg/s, combustion chamber temperature $T_{hc} = 1321$ K and ambient temperature of $T_0 = 288$ K. Additionally, the regenerator effectiveness is defined at $\varepsilon_r = 0.85$. Concerning the overall pressure losses in the heat absorption or dissipation processes, values representing approximately 8% are considered, giving pressure drop coefficients $D_{ps} = D_{pi} = 0.92$. Likewise, other parameters as the heat exchanger's effectiveness, are $\varepsilon_{is} = 0.8$, and $\varepsilon_{ic} = 1$. The latter implies all the heat available at the outlet of the regenerator, which is released to the environment, assuming an open cycle. Similarly, the isentropic efficiencies of the compressor and turbine are $\eta_c = 0.77$ and $\eta_t = 0.85$, respectively. All the above parameters were taken from [47,48].

Table 1 shows the values obtained for the validation with two compressions stages and one expansion stage. A good fit between the results obtained in this work and the references used is observed. Regarding the power results, differences of 1.1% and 0.08% are presented concerning the data of Sanchez Orgaz [47] and Romier [48], respectively. Meanwhile, the thermal engine efficiency η_{hs}presents differences of 1.3% and 3.5%. Finally, the total heat supplied presents a difference of 0.3% for the work of Sanchez Orgaz [47].

Finally, a validation of the model is performed for the case with an expansion stage $N_t$and a compression stage N_c considering a radiation $I_{bh} = 860$ W/m^2. The data for the simulation and the comparison values can be found in [20]. This comparison is presented in Table 2, where an excellent fit of the model data with the real ones can be observed for the overall plant efficiency η, solar fraction f and the solar receiver output T_4. For these values, the highest difference is given for the fuel consumption $\dot{m}_f$ of 2.3% while the others are lower.

3.3. Working fluids evaluated

This work aims to perform a purely thermodynamic comparative analysis of the plant for different working fluids, i.e., air, helium, and carbon dioxide. For instance, supercritical carbon dioxide cycles are presented as a very competitive option because of their high efficiency, equipment size, and less work required in the compressor compared to other working fluids due to the high density and low compressibility of the CO_2 near the critical point [50]. A limitation that may exist in carbon dioxide cycles is the maximum temperature. In this sense, studies of possible reactions of the fluid with the materials have been carried out to reduce this possibility at maximum temperatures around 900 K [51]. Another fluid that is expected to be helpful in closed systems is helium, whose main characteristic is that its specific heat at constant pressure is approximately four times greater than that of air, meaning that enthalpy and temperature changes are also more significant [23]. However, helium cycles present difficulties in the size and shape of shafts and blades that have yet to be solved [52].

From an energetic and exergetic multi-stage analysis, the plant operation performance evaluation through an average day of the year and the search for the best-operating conditions in Barranquilla, Colombia, is required. Given the above, aspects of turbomachines' design, such as the number of steps, size and profiles of blades and shafts, are not evaluated in detail. As Olumayegun et al. [53] described, the same irreversibilities are assumed for all cycles, as are pressure and mass flow relations. The carbon dioxide cycle is set up under the same air cycle operating conditions selected for Barranquilla and is referred to in the following sections as the subcritical carbon dioxide cycle (CO_2),

Table 1
Validation of the model with the turbine manufacturer's data.

	Model	Sanchez Orgaz [47]		Romier [48]	
	Value	Value	Variation (%)	Value	Variation (%)
η_h	0.375	0.37	1.3	0,362	3.5
$\dot{W}_{net}$ (kW)	350.3	346.1	1.2	350	0.08
$\dot{Q}_h$ (kW)	931	928.1	0.3	–	–

Table 2
Validation of the model with data estimated in the literature.

	η	f	T_4 (K)	$\dot{m}_f$ (kg/s)
Estimated Model	0.298	0.337	1042	0.176
Reference [20]	0.300	0.341	1027	0.172
Deviation%	0.06	1.1	1.4	2.3

where the properties used correspond to the Modelica Media Single Gases CO2 library model [54]. Regarding the helium cycle, the pressure ratio must be limited concerning the regenerator operation since at values of r_p higher than 9.9 the inequality $T_6 > T_2$ is not satisfied. The $p - T$ diagram is presented in Fig. 4 for the different working fluids evaluated in the actual work, allowing us to observe that the turbine outlet temperature remains lower than the compressor inlet temperature in the helium cycle. The Helium cycle uses the He properties model from the Coolprop library [60].

Fig. 4 presents the pressure-temperature diagram; it is possible to observe that both the inlet temperature to the compressor T_1 and the turbine T_5 are similar for all working fluids. However, the outlet temperatures of the compressor T_2 and the turbine T_6 change significantly depending on each fluid, particularly in the helium cycle where T_6 is lower than T_2. Furthermore, it can be confirmed that the cycle that operates with carbon dioxide is subcritical, while the cycle that operates with helium is transcritical.

4. Energy and exergy analysis of the hybrid solar thermal plant

This section presents the simulation results of the cycles described in the previous section using different working fluids. The following subsections present the results obtained for the energy analysis of the plant in Barranquilla-Colombia after applying the DI radiation model and the thermodynamic model of the hybrid solar thermal plant validated, as shown in the previous section. Firstly, a comparative analysis of different energy parameters such as net power, overall plant efficiency, fuel consumption and fuel conversion rate of the plant operating with the mentioned fluids is presented. Finally, an exergy evaluation of the hybrid solar thermal plant is presented.

4.1. Solar radiation conditions in Colombia

The plant's operating conditions with ambient temperature and solar radiation in Barranquilla are presented. Subsequently, the influence of the pressure ratio on the power, overall efficiency and fuel conversion rate is evaluated to find the optimum performance point. For the simulation of the plant under the conditions of the city mentioned above, the annual average values of $\overline{H}_h = 6.24$ kWh/m^2/day, $\overline{D}_h = 1.68$ kWh/m^2/day [42], for an annual average day $n = 180$ are used. Barranquilla's hourly average temperature values are taken from [55] to agree with the solar resource estimation. Finally, the value of $Q_{lhv} = 42,624$ kJ/kg is taken from the natural gas quality report of Gas Natural S. A. ESP.

4.2. Plant energy analysis with $N_c \neq N_t$

Brayton cycle configurations may have different compression and expansion stages, resulting in different performances. Therefore, this section introduces four configurations and their respective designation presented by [56], in which *C* refers to compressor, *I* cooling, *T* turbine, *B* reheating, and *X* regeneration.

The pressure ratio significantly impacts the gas turbine operation. In this regard, simulations were developed with an average ambient temperature of 300.03 K and a pressure ratio of 2 – 20 to account for the latter's variable impact on net power, plant efficiencies, and the three working fluids mentioned above. Fig. 5(a) shows the variation of power concerning r_p for the configurations operating with air; it is observed

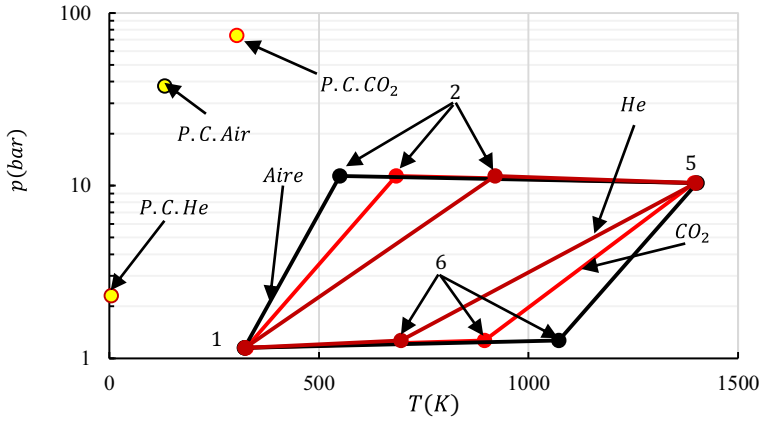

Fig. 4. *p-T* diagram of the cycles with the different conditions to be simulated.

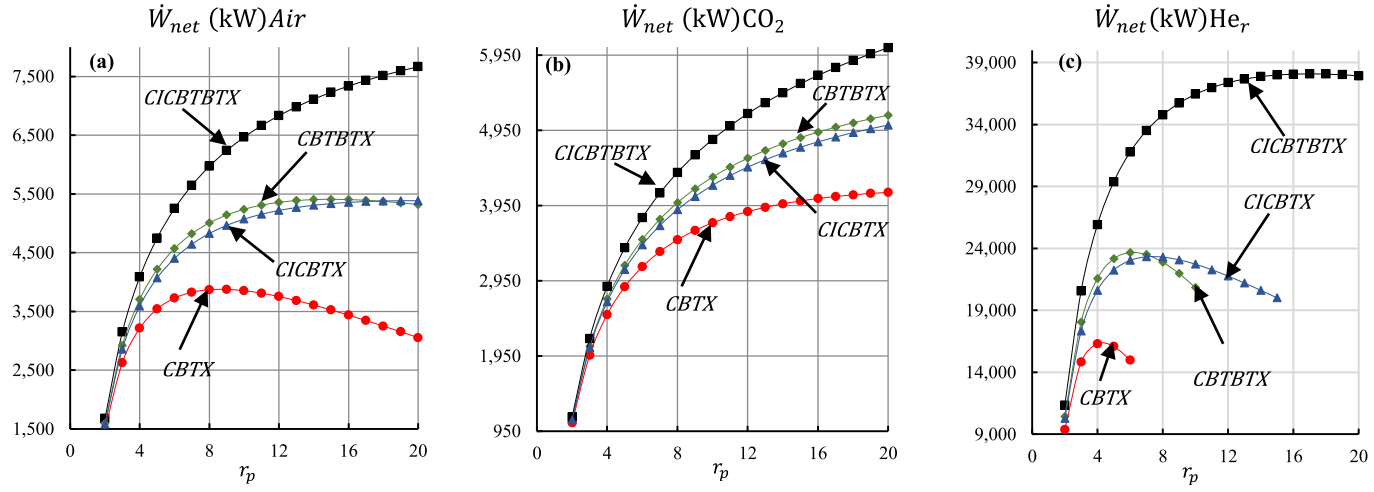

Fig. 5. Evolution of the power of the different configurations as a function of the pressure ratio for the cycle with air (a), carbon dioxide (b) and helium (c).

that the *CBTX* configuration presents the lowest power values in the pressure ratio range, reaching the maximum at r_p= 8.6, the maximum power values and their respective r_p are shown in Table 3. On the other hand, the *CICBTBTX* and *CICBTX* configurations present a continuous growth of net power output over the range of pressure ratios evaluated, producing the maximum value of $\dot{W}_{net}$ for overall pressure ratios greater than 20. Additionally, the *CBTBTX* cycle presents slightly higher power values than the *CICBTX* configuration at low r_p values. However, the *CBTBTX* configuration finds its maximum power at r_p=15 and then declines. Fig. 5(b) presents the influence of the pressure ratio on the configurations operating with CO_2, with higher values for the *CICBTBTX* configuration and lower values for the *CBTX* cycle. Also, the *CBTBTX* cycle presents slightly higher power values than the *CICBTX* cycle and, over the entire pressure ratio range, the curves are monotonically ascending. Additionally, Fig. 5(c) shows the limitation of the pressure ratio in the regenerator's operation when the cycle uses helium. Therefore, only operating data were taken such that the inequality $T_6 > T_2$ is satisfied. This does not allow estimating the power values for the whole r_p range. However, the highest power values are observed for the *CICBTBTX* configuration and the lowest for the *CBTX* cycle, with maximum r_p values of 17 and 4.3, respectively. Additionally, the *CBTBTX* cycle presents slightly higher power values than the *CICBTX* configuration at low r_p values. However, the *CBTBTX* configuration finds its maximum power at r_p= 6.2 and then declines rapidly, allowing the power values of the *CICBTX* configuration to be higher from a pressure ratio of 7 onwards.

The *CICBTBTX* configuration presents the highest power values, and the *CBTX* configuration generates the lowest power. The same occurs with the overall efficiency when f_{max} at noon, it is shown in Fig. 6. The

Table 3
Maximum power and global efficiency values for each configuration.

	Power ($\dot{W}_{net}$)						Overall efficiency (η)					
	Air		CO_2		He_r		*Air*		CO_2		He_r	
Cycle	r_p	*P*(*kW*)	r_p	*P*(*kW*)	r_p	*P*(*kW*)	r_p	η	r_p	η	r_p	η
CBTX	8.6	3875	>20	–	4.3	16,366	6.3	0.27848	15.4	0.28783	3.4	0.29298
CICBTX	>20	–	>20	–	7.4	23,339	10.5	0.32661	>20	–	4.7	0.34337
CBTBTX	15	5407	>20	–	6.2	23,673	8.3	0.30257	>20	–	4.1	0.32042
CICBTBTX	>20	–	>20	–	17	38,083	18.9	0.36185	>20	–	6.7	0.38021

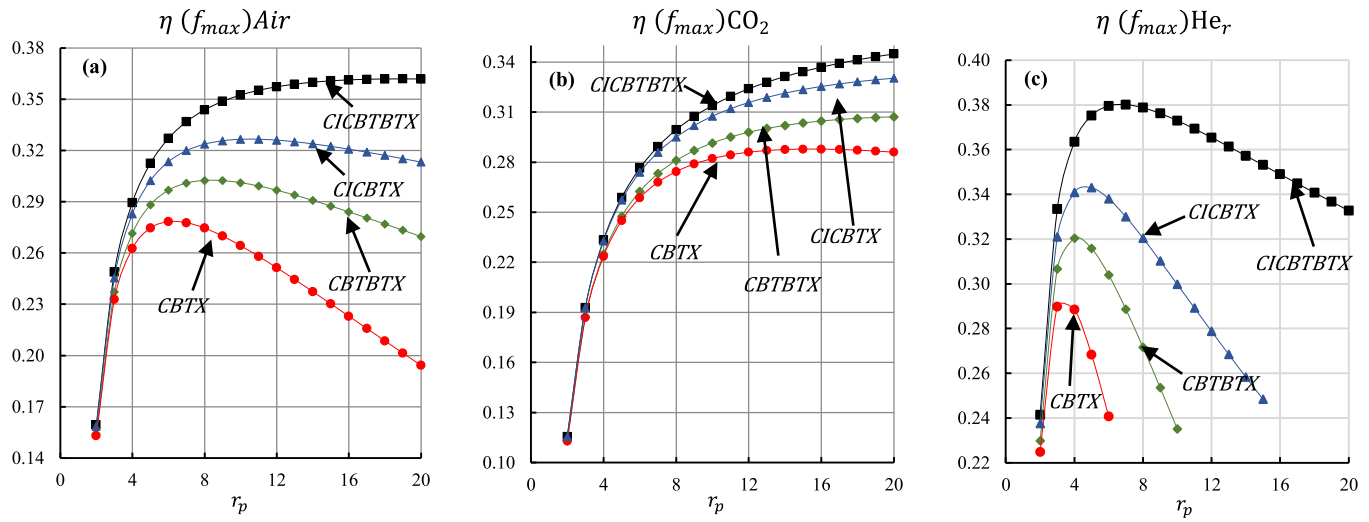

Fig. 6. Evolution of the overall efficiency of the different configurations when (f_{max}) as a function of the pressure ratio for the cycle with air (a), carbon dioxide (b) and helium (c).

CBTX configuration maintains a higher value of η, due to its lower fuel consumption. For each working fluid, it is observed that the cycles of lower overall efficiency also reduce the pressure ratio value of the maximum efficiency point. Additionally, in the cycles with CO_2 (see Fig. 6(b)), only the *CBTX* cycle presents its maximum overall efficiency in the evaluated r_p range ($r_p = 15.4$) and then declines slightly. The other configurations increase their overall efficiency monotonically at r_p values between zero and 20. This can be seen in Table 3, where the maximum values of overall efficiency for all configurations are presented with the respective pressure ratio value where this maximum value is found. Helium cycles have better efficiency at low-pressure ratios and then decrease drastically.

From the evolution of the cycle's net power as a function of the r_p, it is observed that the values of $\dot{W}_{net}$ are higher for air concerning CO_2, especially at low values of r_p. However, these values decrease as r_p increases for the cycle using air, while in the case of CO_2 they tend to grow continuously [27]; this difference is due to the higher CO_2 specific heat value concerning other working fluids [23], allowing its application at higher pressure ratio values [57]. The global efficiency behaviour is similar to the observed in the case of the net power for air and CO_2, however, the helium presents a high specific heat value, which allows it to deliver more significant amounts of work, but at the same time, requires a higher energy input reflected in significant increases in fuel consumption [23]. Additionally, it presents significant changes in the temperature at the outlet of the compressor and the turbine, which reduces the option of using a regenerator in a gas turbine with helium as a working fluid. Additionally, it is observed that the cycles with helium present their best performance at lower r_p values with several stages of compression and expansion, which agrees with the results presented by Merchán et al. [58].

Fig. 7 shows the overall plant's efficiency evolution, where it is observed that the *CICBTBTX* and *CBTX* configurations present the highest and lowest overall efficiency (e.g., with values at midday equal to 0.3532 and 0.2665, respectively), corresponding to the value of net power delivered. However, in the *CICBTX* configuration, the overall efficiency presents a value of 0.3277 for f_{max}, which is higher for *CBTBTX* (i.e., 0.3026 when f_{max}), even though the latter configuration produces 3.3% more power under the described operating conditions. This variation is because the intermediate reheating of the *CBTBTX* configuration increases the total fuel consumption of the plant and, therefore, reduces its overall efficiency.

Regarding the configurations with air, all of them have a maximum η in the range of pressure ratios studied, as shown in Fig. 7 and whose

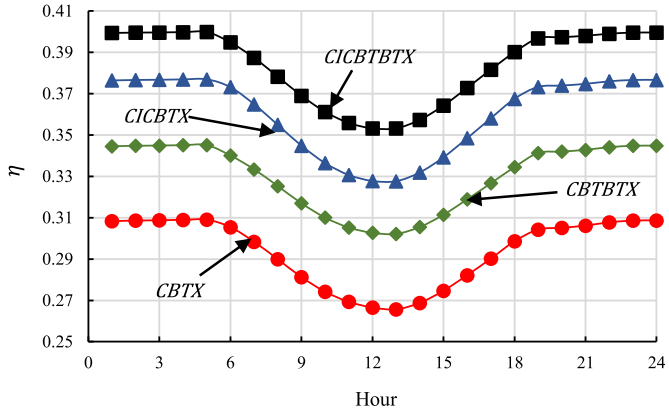

Fig. 7. Overall efficiency evolution of *CBTX,CICBTBTX, CICBTX* and *CBTBTX* configurations operating with air.

values can be seen in Table 3. After the maximum point, the efficiency of the air configurations decreases and tends to be surpassed by the CO_2 cycles except for the *CICBTBTX* configuration whose efficiency is always higher for the cycle operating with air than that of CO_2. Cycles with He_r have the highest maximum values of η, but these maximum values are found at low-pressure ratios (see Table 3).

As the solar resource increases, the amount of heat supplied to the cycle by the concentrating solar system also increases, represented by an increase in the solar factor (f) and a corresponding fuel consumption reduction [19]. However, the solar concentration system has significant heat losses that reduce the efficiency of the plant, especially when the solar resource is maximum (f_{max}) [59]. In the present work, an analysis of the solar factor is not presented, given the number of configurations and working fluids. However, the evolution of f for the *CBTX* configuration is presented by Moreno-Gamboa et al. in [6], where it was observed that under the same conditions, f is much lower for the helium cycle, due to the large amount of energy needed by the system and the concentrator is noted undersized [58].

The fuel conversion rate does not represent thermodynamic efficiency; it measures system performance from the point of view of fuel consumption costs [34]. In this sense, it can be observed that the CO_2 cycles present values slightly higher than the air cycles due to their lower fuel consumption. In contrast, despite its large power values, the helium cycle's values are lower due to its higher fuel consumption.

Finally, the fuel conversion rate r_e is evaluated for the previously analysed configurations and fluids. Fig. 8 presents the variations of r_e concerning the pressure ratio for the maximum solar fraction, the condition (f_{max}). As previously verified, fuel consumption is strongly influenced by the turbine outlet temperature T_6, which in turn is related to the regenerator outlet temperature T_3, the combustion chamber outlet T_6, and the inlet temperature at each of the reheaters. It can be observed that for the cycles operating with air and CO_2 at low-pressure ratios, the *CICBTX* and *CBTX* cycles present the highest economic performance values. This is expected because both configurations do not present overheating, and the turbine inlet temperature T_6 is higher compared to the other configurations. However, after the maximum point (see Table 4), they rapidly decrease, presenting lower economic performance than the *CBTBTX* and *CICBTBTX* cycles when operating with air, which present higher net power values for that pressure range. Additionally, the maximum values of the economic performance for these cycles occur for pressure ratio values close to where the maximum cycle performances occur (see Tables 4 and 3). The *CICBTX* configuration using CO_2 presents the highest values of r_e at its maximum point (*PM*) over most of the r_p range evaluated.

The variation of r_e in the cycles with He_r is different, mainly due to the enormous changes in the turbine and compressor outlet temperature with the pressure ratio. It is possible to observe that the *CICBTBTX* configuration presents the highest efficiency and the *CBTX* cycle the lowest. Additionally, in the cycles with He_r the maximum r_e values (see Table 4), occur for a pressure ratio range between 3.4 and 6.2, while the air cycles present their maxima in an r_p range between 4.7 and 9.4.

4.3. Exergy analysis of the hybrid solar thermal plant

This section presents the exergy analysis of the different plant configurations and working fluids; the model allows studying different configurations throughout the day. Fig. 9 shows the evolution of the total exergy destruction of the configurations when these configurations operate with air as a working fluid, where the variation of the total exergy destruction of these configurations throughout the day is presented. It can be observed that the combustion chamber configurations with reheating (i.e., *CICBTBTX*and*CBTBTX*) tend to destroy more exergy than those without, with an average difference between both configurations of 0.6%. Additionally, the CBTBTX configuration destroys more exergy by having only one compressor that increases the air temperature before the regenerator; therefore, it destroys more exergy in the heat exchange with the environment. Likewise, the *CBTX* configuration, which also has a single compressor, destroys, on average 0.7% more exergy than the *CICBTX* configuration, the latter being the configuration that destroys the least total exergy.

Table 4
Maximum fuel conversion rate values for each configuration.

	Fuel conversión rate (r_e)					
	Air		CO_2		He_r	
Cycle	r_p	r_e	r_p	r_e	r_p	r_e
CBTX	4.7	0.46986	9.7	0.47479	3.4	0.32546
CICBTX	6.6	0.50679	16.3	0.51057	4.7	0.37486
CBTBTX	5.6	0.45514	12.4	0.4569	3.9	0.34803
CICBTBTX	9.4	0.49760	>20	–	6.2	0.40549

The evolution of the overall exergy efficiency of the configurations throughout the day is shown in Fig. 10. The *CICBTBTX* and *CBTX* configurations show the highest and lowest overall efficiency (with values when f_{max} at midday of 0.324657 and 0.24882, respectively), corresponding to the value of the net power delivered. However, in the *CICBTX* configuration, the overall efficiency presents a value of (0.304563 for f_{max}), which is higher than *CBTBTX* (0.279119 in f_{max}), despite the latter configuration producing 3.3% more power under the described operating conditions. This variation is because the intermediate reheating of the *CBTBTX* configuration increases the total fuel consumption of the plant and therefore reduces its overall efficiency.

Evaluating the exergy destruction is essential to define which plant components destroyed the most exergy and evaluate its improvement possibilities. In this sense, the fraction of exergy destruction in the different components of the plant configurations when operating with air as a working fluid is presented. Fig. 11 shows the variation of the fraction of exergy destruction concerning the total exergy destroyed in each component, where it is observed that during the night hours, the variation of each fraction is minimal. This changes when the solar resource becomes available, which increases the exergy destruction in the components and reduces that of the others, especially in the main combustion chamber, due to the reduction of heat supply in this component. Fig. 11(a) shows the exergy destruction of the components of the CBTX configuration, where it can be observed that for f_{max}, the fraction of exergy destruction in the heliostat field reaches a maximum of 0.1891 and 0.05418 in the receiver.

On the other hand, the fraction of exergy destruction decreases in the other components, especially in the combustion chamber, where it is reduced by 34.6%, the component that destroys the most exergy, followed by the heat exchanger with the environment. In the other components, the reduction of the exergy destruction fraction is around 10%. Additionally, Fig. 11(b) shows the exergy destruction fraction in the

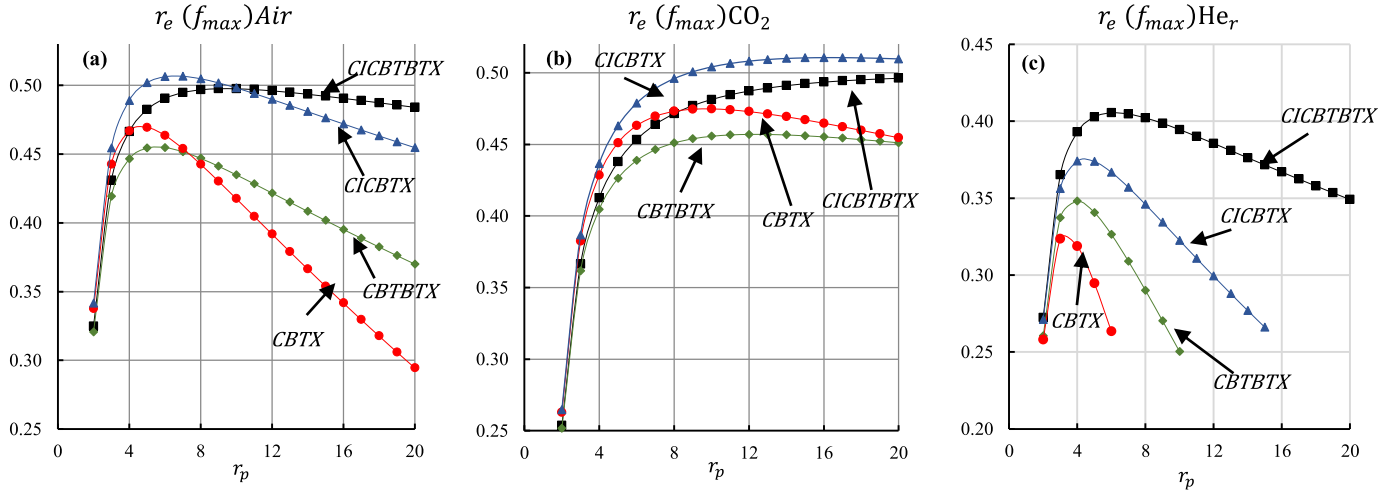

Fig. 8. Evolution of the fuel conversion rate of the different configurations when (f_{max}) as a function of the pressure ratio for the cycle with air (a), carbon dioxide (b) and helium (c).

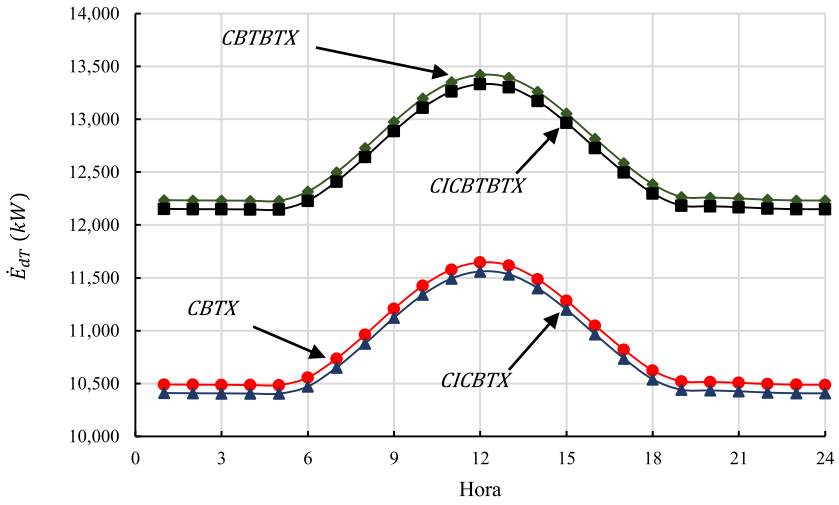

Fig. 9. Evolution of total exergy destruction of *CBTX, CICBTBTX, CICBTX* and *CBTBTX* configurations, operating with air.

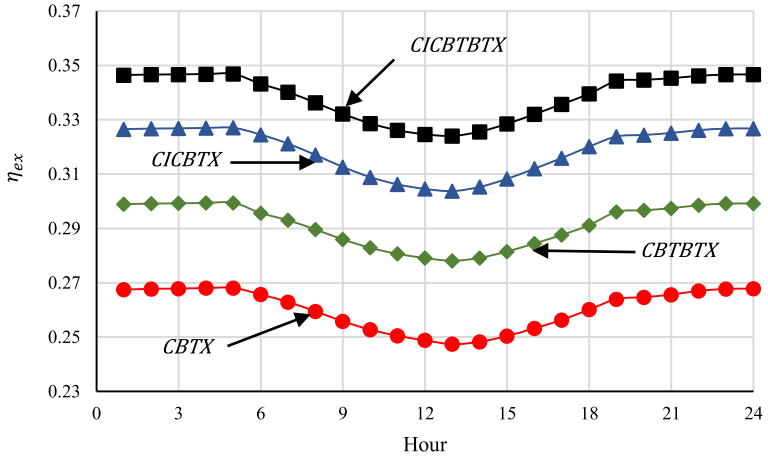

Fig. 10. Evolution of total exergy efficiency of CBTX, CICBTBTX, CICBTX and CBTBTX configurations, operating with air.

CICBTX configuration, where it can be observed that no exergy destruction occurs during reheating since the cycle has only one turbine. The most significant heat input is in the main combustion chamber, which has an exergy destruction fraction $F\dot{E}_{d,cc}$ of 0.64 when the solar factor is zero and 0.429 when *f* is maximum. On the other hand, since the cycle has two compressors, the exergy destruction fraction in the intermediate cooling $F\dot{E}_{d,aem}$ and the heat exchanger $F\dot{E}_{d,a}$ represent an average fraction of 0.188. The solar concentration system represents a maximum fraction of 0.25 at noon.

Regarding the components' exergetic analyses of all configurations, it is observed that the combustion processes in the combustion chamber and overheating combustion chambers represent the highest fractions of typical exergy destruction in these components [60]. The process was also evaluated with excess air of 300% [40] and heat exchangers. In this sense, it is essential to evaluate the reduction of exergy destruction by analysing the chamber temperature and the overheating and excess combustion air.

Regarding the *CBTBTX* configuration, Fig. 11(c) shows that the exergy destruction in the reheater $F\dot{E}_{d,ccrm}$ and the main combustion chamber $F\dot{E}_{d,cc}$ account for a total fraction of 0.57 on average when the solar factor is zero. This value is reduced to 0.4 when *f* is the maximum. For this configuration, the fraction of exergy destruction in the heat exchanger with the environment $F\dot{E}_{d,a}$, represents, on average, a fraction of 0.30. It can also be noted that no exergy destruction occurs in the intermediate cooling since there is only one compressor. Additionally, the solar concentration system has a maximum fraction of 0.1979. Finally, Fig. 11(d) shows the fraction of exergy destruction in the components of the *CICBTBTX* configuration, where it can be seen that both the reheating between turbines and the intermediate cooling between compressors appear. Also, it is observed that the exergy destruction in the reheater $F\dot{E}_{d,ccrm}$ and the main combustion chamber $F\dot{E}_{d,cc}$ represent a total fraction of 0.624 on average when the solar factor is zero and reduces to 0.453 when *f* is maximum at midday. Also, it is observed that the exergy destruction in the reheater $F\dot{E}_{d,ccrm}$ and the main combustion chamber $F\dot{E}_{d,cc}$ represent a total fraction of 0.624 on average when the solar factor is zero and reduces to 0.453 when *f* is maximum at midday.

Fig. 12 shows the variations in the global exergy efficiency η_{ex} concerning the global pressure ratio $r_p$when the solar fraction is maximum. The configurations with air as the working fluid are presented in Fig. 12 (a). The maximum value (see Table 5) of all the configurations is found in the range of r_p 6.1 and 17.4. The *CICBTBTX* configuration presents the highest values of η_{ex}; furthermore, the *CBTX* configuration has the lowest values of overall exergy efficiency. Regarding the plant using CO_2 (see Fig. 12(b)), it can be seen that in the *CICBTX, CBTBTX* and *CICBTBTX* configurations, the η_{ex}values show continuous growth in the r_p range between 2 and 20. However, the *CBTX* configuration presents its maximum at $r_p = 14.7$ (see Table 5). Additionally, configurations with He$_r$(see Fig. 12(c)) present maximum values of η_{ex} in a pressure ratio range between 3.4 and 6.6.

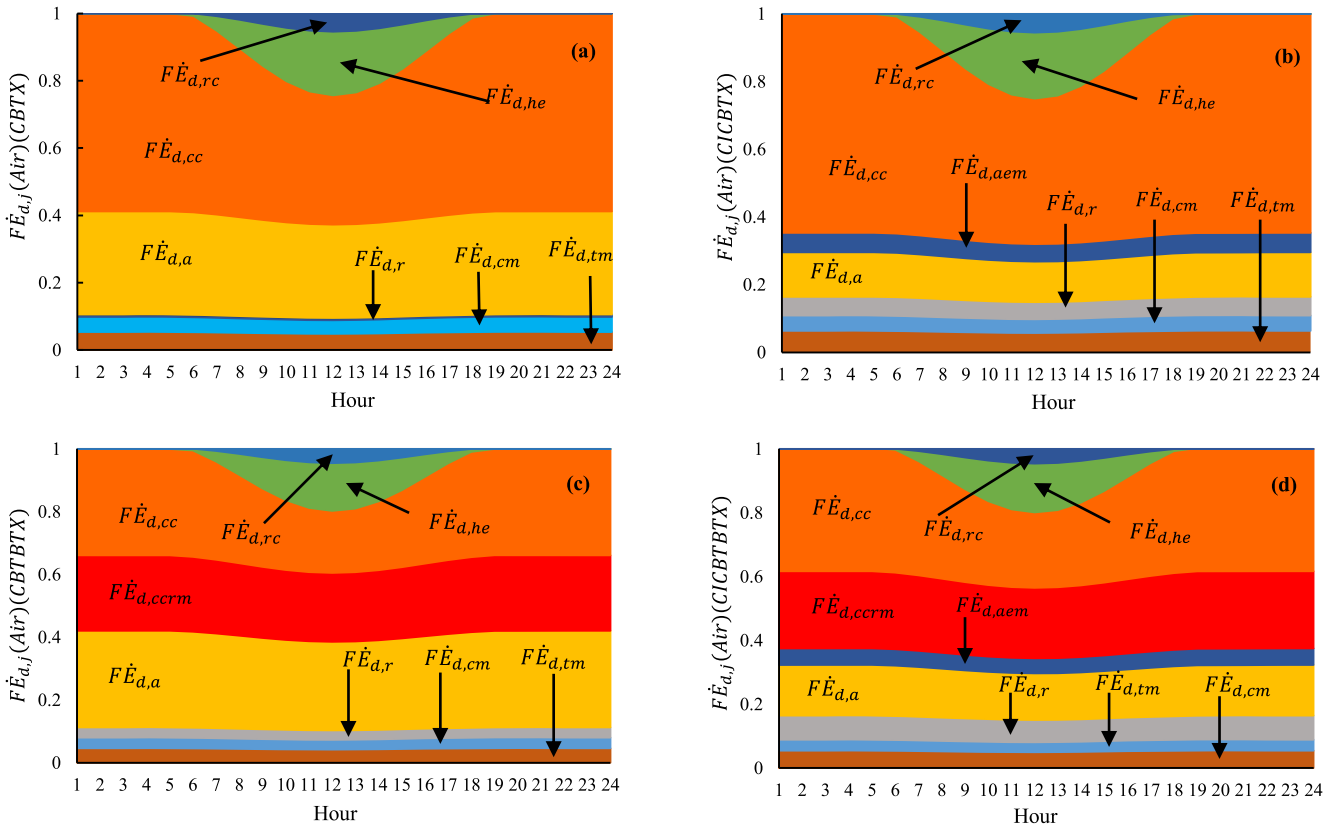

Fig. 11. Evolution of the exergy destruction fraction when the plant operates with *Air* in *CBTX* (a), *CICBTX* (b), *CBTBTX* (c), and *CICBTBTX* (d) configurations.

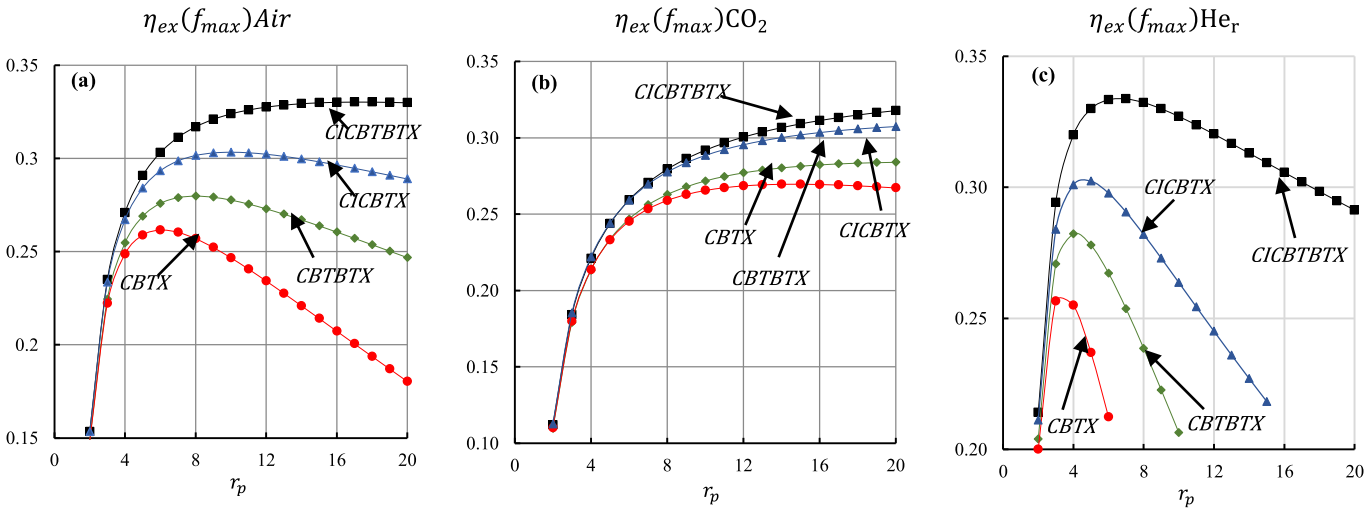

Fig. 12. Evolution of overall exergy efficiency for air (a), CO_2 (b) and He_r cycles (c).

Table 5
Maximum global exergy efficiency values for each configuration.

	Global exergy efficiency (η_{ex})					
	Air		CO_2		He_r	
Cycle	r_p	η_{ex}	r_p	η_{ex}	r_p	η_{ex}
CBTX	6.1	0.26158	14.7	0.2696	3.4	0.25916
CICBTX	10	0.30337	>20	–	4.6	0.30280
CBTBTX	8	0.27979	>20	–	4.1	0.2822
CICBTBTX	17.4	0.33028	>20	–	6.6	0.33383

In the solar concentrator, it is expected that the most significant destruction of exergy occurs in the heliostat field [57], despite using, in this case, an optical efficiency of 0.73 [36], although some authors recommend lower values or take into account the effects of heliostat field configuration, location, and distribution [61]. For the working fluids, the high fuel consumption of re-related helium cycles and the higher heat transfers within the cycle significantly reduce exergy destruction and exergetic efficiency.

5. Conclusions

The model allows its application to places where measured radiation data are unavailable, such as Barranquilla. This paper presents and validates a thermodynamic model used in hybrid Brayton cycle plants with a central tower concentrating system coupled to a solar resource estimation model and an arbitrary number of compression and expansion stages, including the analysis of exergy destruction. The analysis can be performed for different times of the day and different plant configurations. The model also allows evaluating configurations with different compression and expansion stages from an energetic and exergetic point of view. For the four configurations evaluated operating with air as working fluid, it is observed that for the operating conditions when $r_p = 9.9$, the configuration with the highest power is the *CICBTBTX*, whose power is 67.9% higher than the *CTBX* configuration, followed by the *CBTBTX*, which tends lowering its performance at high-pressure ratio values.

Regarding the overall efficiency η, the *CICBTBTX* configuration is still the one with the highest values, reaching 40% more than the *CTBX* configuration. The second-highest efficiency configuration is the *CICBTX* due to its lower fuel consumption; the reheating causes the *CBTBTX* configuration to deliver lower efficiency than the *CICBTX* configuration. In general, the *CBTX* configuration has the lowest power and efficiency. Additionally, it is observed that economic efficiency, r_e, is higher in the CICBTX cycle with air for values of $r_p < 10$. On the other hand, the CO_2 cycle presents a higher r_e for the whole range of r_p evaluated. The helium cycle presents the lowest r_e values, including all configurations, given the high fuel consumption. From this point of view, the subcritical carbon dioxide cycles for the *CICBTX* configuration are presented as an excellent option in developing this type of plant due to their high efficiency and low fuel consumption.

The *CBTBTX* cycle presents the highest values of total exergy destruction due to the reheating and the use of a single compression stage. This causes the regenerator outlet temperature $T_7$to be higher, thus increasing the exergy destruction in the heat transfer to the environment. On the other hand, the *CICBTX* cycle is the cycle that destroys less exergy because no reheating occurs. As a result, less exergy is destroyed in releasing heat to the environment.

In the comparative analysis of the operation of different working fluids, it is observed that helium can achieve important net power values and efficiencies at low-pressure ratios due to its high specific heat and adiabatic coefficient, but its performance is affected as r_p increases, and consequently, its performance when operating with multiple stages of expansion and compression. However, the helium cycle is characterised by higher fuel consumption, and when compared with the same solar power system with other working fluids, its power increase diminishes due to the significant amount of heat required for its operation that the working fluid requires. Meanwhile, the CO_2 cycles consume less fuel than the air cycle, with the corresponding increase in efficiency and the ability to perform better in a wide range of pressure ratios.

Emphasising that the input operation parameters were the same for the different configurations, future works must evaluate the cycles and their working fluids at their best power and efficiency points, considering possible restrictions of each fluid, such as their maximum temperature. Additionally, it is essential to complete the model with an analysis of levelized energy costs, which allows for studying the configurations from technical and economic points of view.

Declaration of Competing Interest

The authors declare that they have no known competing financial interests or personal relationships that could have appeared to influence the work reported in this paper.

Data availability

Data will be made available on request.

Acknowledgements

The authors would like to thank Universidad Francisco de Paula Santander for providing the computer equipment, the Dymola license, and the doctoral studies commission of the author Faustino Moreno.

References

[1] M. Santhosh, C. Venkaiah, D.M. Vinod Kumar, Current advances and approaches in wind speed and wind power forecasting for improved renewable energy integration: a review, Eng. Reports 2 (6) (2020) 1–20.
[2] H. Aljaghoub, F. Abumadi, M.N. AlMallahi, K. Obaideen, A.H. Alami, Solar PV cleaning techniques contribute to sustainable development goals (SDGs) using multi-criteria decision-making (MCDM): assessment and review, Int. J. Thermofluids 16 (October) (2022), 100233.
[3] S. Dmitry, S. Liubov, Numerical modelling of heat accumulator performance at storage of solar energy, Int. J. Thermofluids 17 (December 2022) (2023), 100268.
[4] F. Moreno-Gamboa, C. Nieto-Londoño, Hybrid Brayton multi-stage concentrated solar power plant energy and exergy performance study, J. Energy Resour. Technol. 143 (6) (2021).
[5] S.C. Kaushik, V.S. Reddy, S.K. Tyagi, Energy and exergy analyses of thermal power plants: a review, Renew. Sustain. Energy Rev. 15 (4) (2011) 1857–1872.
[6] F. Moreno-Gamboa, A. Escudero-Atehortua, C. Nieto-Londoño, Alternatives to improve performance and operation of a hybrid solar thermal power plant using hybrid closed Brayton cycle, Sustainability 14 (15) (2022) 9479.
[7] REN 21, "Renewables 2021, global status report," 2021.
[8] S. Guo, Q. Liu, J. Sun, H. Jin, A review on the utilisation of hybrid renewable energy, Renew. Sustain. Energy Rev. 91 (2018) 1121–1147. Elsevier Ltd01-Aug-.
[9] M. Quero, R. Korzynietz, M. Ebert, A.A. Jiménez, A. Río, J.A. Brioso, Solugas – operation experience of the first solar hybrid gas turbine system at MW scale, Energy Procedia 49 (2014) 1820–1830.
[10] M.T. Dunham, B.D. Iverson, High-efficiency thermodynamic power cycles for concentrated solar power systems, Renew. Sustain. Energy Rev. 30 (2014) 758–770.
[11] T.K. Ibrahim, et al., Thermal performance of gas turbine power plant based on exergy analysis, Appl. Therm. Eng. 115 (2017) 977–985. Mar.
[12] P.E.B. de Mello, D.B. Monteiro, Thermodynamic study of an EFGT (externally fired gas turbine) cycle with one detailed model for the ceramic heat exchanger, Energy 45 (1) (2012) 497–502. Sep.
[13] E. Jansen, T. Bello-Ochende, J.P. Meyer, Integrated solar thermal Brayton cycles with either one or two regenerative heat exchangers for maximum power output, Energy 86 (2015) 737–748. Jun.
[14] M.K. Sahu, Sanjay, Thermoeconomic investigation of basic and intercooled gas turbine based power utilities incorporating air-film blade cooling, J. Clean. Prod. 170 (2018) 842–856. Jan.
[15] M.K. Sahu, Sanjay, Thermoeconomic investigation of power utilities: intercooled recuperated gas turbine cycle featuring cooled turbine blades, Energy 138 (2017) 490–499. Nov.
[16] T. Nada, Performance characterisation of different configurations of gas turbine engines, Propuls. Power Res. 3 (3) (2014) 121–132. Sep.
[17] S. Sanaye, M. Amani, P. Amani, 4E modeling and multi-criteria optimisation of CCHPW gas turbine plant with inlet air cooling and steam injection, Sustain. Energy Technol. Assessments 29 (2018) 70–81. Oct.
[18] P. Heller, et al., Test and evaluation of a solar powered gas turbine system, Sol. Energy 80 (10) (2006) 1225–1230. Oct.
[19] D. Olivenza-León, A. Medina, A.Calvo Hernández, Thermodynamic modeling of a hybrid solar gas-turbine power plant, Energy Convers. Manag. 93 (2015) 435–447.
[20] M.J. Santos, R.P. Merchán, A. Medina, A.Calvo Hernández, Seasonal thermodynamic prediction of the performance of a hybrid solar gas-turbine power plant, Energy Convers. Manag. 115 (2016) 89–102.
[21] M. Livshits, A. Kribus, Solar hybrid steam injection gas turbine (STIG) cycle, Sol. Energy 86 (1) (2012) 190–199. Jan.
[22] G. Barigozzi, A. Perdichizzi, C. Gritti, I. Guaiatelli, Techno-economic analysis of gas turbine inlet air cooling for combined cycle power plant for different climatic conditions, Appl. Therm. Eng. 82 (2015) 57–67. May.
[23] M.J. Santos, C. Miguel-Barbero, R.P. Merchán, A. Medina, A.Calvo Hernández, Roads to improve the performance of hybrid thermosolar gas turbine power plants: working fluids and multi-stage configurations, Energy Convers. Manag. 165 (December 2017) (2018) 578–592.
[24] W. Scheuermann, N. Haneklaus, and M. Fütterer, The high temperature gas-cooled reactor: safety considerations of the (V)HTR-Modul, no. V. 2017.
[25] I.A. Weisbrodt, "Summary report on technical experiences from high temperature helium turbine in Germany. Report IAE-TECDOC-899 Vienna," 1994.
[26] Y. Ding, Status of development and deployment scheme of HTR-PM in the People's Republic of China, in: Interregional Workshop on Advanced Nuclear Reactor Technology for Near Term Deployment, 2011.

[27] Y. Liu, Y. Wang, D. Huang, Supercritical CO2 Brayton cycle: a state-of-the-art review, Energy 189 (2019), 115900.
[28] T. Neises, C. Turchi, A comparison of supercritical carbon dioxide power cycle configurations with an emphasis on CSP applications, Energy Procedia 49 (2014) 1187–1196.
[29] X. Lei, R. Peng, Z. Guo, H. Li, K. Ali, X. Zhou, Experimental comparison of the heat transfer of carbon dioxide under subcritical and supercritical pressures, Int. J. Heat Mass Transf. 152 (2020), 119562.
[30] D. Thanganadar, F. Asfand, K. Patchigolla, Thermal performance and economic analysis of supercritical Carbon Dioxide cycles in combined cycle power plant, Appl. Energy 255 (2019), 113836. Dec.
[31] A. Calvo Hernández, J.M.M. Roco, A. Medina, Power and efficiency in a regenerative gas-turbine cycle with multiple reheating and intercooling stages, J. Phys. D. Appl. Phys. 29 (6) (1996) 1462–1468.
[32] C.A. Gueymard, Prediction and performance assessment of mean hourly global radiation, Sol. Energy 68 (3) (2000) 285–303.
[33] Y. Goswami, Principles of Solar Engineering, 3rd edit, CRC Press Taylor & Francis Group, Boca Raton, FL, 2015.
[34] F. Moreno-Gamboa, A. Escudero-Atehortua, C. Nieto-Londoño, Performance evaluation of external fired hybrid solar gas-turbine power plant in Colombia using energy and exergy methods, Therm. Sci. Eng. Prog. 20 (2020), 100679.
[35] B. Joshi, Thermodynamic work for N-step isothermal processes involving and ideal gas, J. Chem. Educ. 63 (1986) 24–27.
[36] M. Romero, R. Buck, J.E. Pacheco, An update on solar central receiver systems, projects, and technologies, J. Sol. Energy Eng. 124 (2) (2002) 98–109. May.
[37] J. Duffie, W. Beckman, Solar Engineering of Thermal Processes, Fourth Edi, John Wiley & Sons, New Jersey, 2013.
[38] L. Chen, N. Ni, F. Sun, FTT performance of a closed regenerative Brayton cycle coupled to variable-temperature heat reservoir, in: Proceedings of the International Conference on Marine Engineering, 1996, pp. 371–1996.
[39] Y.A. Cengel and M.E. Boles, Thermodynamics: an engineering approach. 2012.
[40] T. Yue, N. Lior, Thermal hybrid power systems using multiple heat sources of different temperature: thermodynamic analysis for Brayton cycles, Energy 165 (2018) 639–665.
[41] R. Petela, Exergy of undiluted thermal radiation, Sol. Energy 74 (February) (2003) 469–488.
[42] N. A. and S. A. (NASA), "Power data access viewer," 2018.
[43] Meteosevilla, "Estacion meterológica santiponce, Sevilla, España." [Online]. Available: www.meteosevilla.com. [Accessed: 25-Jun-2021].
[44] R. Mejdoul, M. Taqi, The mean hourly global radiation prediction models investigation in two different climate regions in Morocco, Int. J. Renew. Energy Res. 2 (4) (2012) 608–617.
[45] W. Yao, Z. Li, T. Xiu, Y. Lu, X. Li, New decomposition models to estimate hourly global solar radiation from the daily value, Sol. Energy 120 (2015) 87–99.
[46] C.A. Gueymard, J.A. Ruiz-Arias, Extensive worldwide validation and climate sensitivity analysis of direct irradiance predictions from 1-min global irradiance, Sol. Energy 128 (2016) 1–30.
[47] S. Sanchez Orgaz, Tesis Doctoral, Univesidad de Salamanca, 2012.
[48] A. Romier, Small gas turbine technology, Appl. Therm. Eng. 24 (11–12) (2004) 1709–1723.
[49] L.E. Herranz, J.I. Linares, B.Y. Moratilla, Power cycle assessment of nuclear high temperature gas-cooled reactors, Appl. Therm. Eng. 29 (8–9) (2009) 1759–1765. Jun.
[50] M. Kulhánek, V. Dostál, Supercritical carbon dioxide cycles thermodynamic analysis and comparison, in: Supercritical CO2 power cycle symposium, 2011.
[51] H.J. Lee, H. Kim, C. Jang, Compatibility of candidate structural materials in high-temperature S-CO2 environment, in: The 4th International Symposium - Supercritical CO2 Power Cycles, 2014, pp. 1–9.
[52] C.F. McDonald, Helium turbomachinery operating experience from gas turbine power plants and test facilities, Appl. Therm. Eng. 44 (2012) 108–142. Pergamon01-Nov-.
[53] O. Olumayegun, M. Wang, G. Kelsall, Closed-cycle gas turbine for power generation: a state-of-the-art review, Fuel 180 (2016) 694–717.
[54] "Modelica.Media.IdealGases.SingleGases.CO2." [Online]. Available: https://build.openmodelica.org/Documentation/Modelica.Media.IdealGases.SingleGases.CO2.html. [Accessed: 21-Mar-2020].
[55] E. Ramírez-Cerpa, M. Acosta-Coll, J. Vélez-Zapata, Análisis de condiciones climatológicas de precipitaciones de corto plazo en zonas urbanas: caso de estudio Barranquilla, Colombia, Idesia (Arica) 35 (ahead) (2017), 0–0.
[56] J.H. Horlock, W.W. Bathie, Advanced Gas Turbine Cycles, 126, 2004.
[57] M.E. Siddiqui, K.H. Almitani, Energy and exergy assessment of s-CO_2 Brayton cycle coupled with a solar tower system, Processes 8 (10) (2020) 1–23.
[58] R.P. Merchán, M.J. Santos, I. Heras, J. Gonzalez-Ayala, A. Medina, A.C. Hernández, On-design pre-optimisation and off-design analysis of hybrid Brayton thermosolar tower power plants for different fluids and plant configurations, Renew. Sustain. Energy Rev. 119 (2020).
[59] R.P. Merchán, M.J. Santos, A. Medina, A.Calvo Hernández, Thermodynamic model of a hybrid Brayton thermosolar plant, Renew. Energy 128 (2018) 473–483.
[60] R.V. Padilla, Y.C. Soo Too, R. Benito, W. Stein, Exergetic analysis of supercritical CO2 Brayton cycles integrated with solar central receivers, Appl. Energy 148 (2015) 348–365.
[61] V. Zare, M. Hasanzadeh, Energy and exergy analysis of a closed Brayton cycle-based combined cycle for solar power tower plants, Energy Convers. Manag. 128 (2016) 227–237.